Modeling Localized Corrosion of Corrosion-Resistant Alloys in Oil and Gas Production Environments: Part I. Repassivation Potential

A. Anderko,‡, F. Gui,** L. Cao,** N. Sridhar,** and G.R. Engelhardt**

ABSTRACT

A model has been developed for predicting the localized corrosion repassivation potential (E_{rp}) for alloys in environments containing chloride ions and hydrogen sulfide. The model has been combined with E_{rp} measurements for a 13-Cr supermartensitic stainless steel (UNS S41425) at various concentrations of Cl^- and H_2S. The model accounts for competitive adsorption at the interface between the metal and the occluded site environment, the effect of adsorbed species on anodic dissolution, and the formation of solid phases in the process of repassivation. The effect of H_2S is complex, as it may give rise to a strong enhancement of anodic dissolution in the occluded environment and may lead to the formation of solid metal sulfide phases, which compete with the formation of metal oxides. H_2S can substantially reduce the repassivation potential, thus indicating a strongly enhanced tendency for localized corrosion and stress corrosion cracking. However, exceptions exist at lower H_2S and Cl^- concentrations, at which H_2S may lead to the inhibition of localized corrosion. The model accurately reproduces the measured repassivation potentials for Alloy S41425 and the limited literature data for Alloy CA6NM (UNS J91574), thus elucidating the conditions at which H_2S increases the propensity for localized corrosion and those at which it does not. Because the repassivation potential defines the threshold condition for the existence of stable pits or crevice corrosion, the model provides the foundation for predicting localized corrosion and stress corrosion cracking in environments that are relevant to oil and gas production.

KEY WORDS: corrosion-resistant alloys, hydrogen sulfide corrosion, localized corrosion, repassivation potential, stress corrosion cracking

INTRODUCTION

Corrosion behavior of corrosion-resistant alloys (CRAs) in the oil and gas industry has been attracting significant attention over the past two decades as a result of a marked trend toward increasing severity of corrosive environments in terms of temperature, pressure, and aggressive species. This trend, coupled with increasing scrutiny of production systems by regulators and the public, is expected to continue in the future and provides impetus to a reexamination of approaches to materials selection.

At present, materials specification is based on a combination of standard tests (e.g., NACE TM-01-77[1]), fit-for-purpose testing, and experience. The empirical knowledge is embodied in standards, such as ISO 15156,[2] guidance documents, and company specifications. The boundaries of acceptable performance of CRAs are often specified in terms of empirically determined ranges of H_2S and CO_2 partial pressures. However, such approaches may not be satisfactory because the performance of CRAs depends on many other factors such as temperature, acidity, chloride concentration, elemental sulfur, etc., which in turn may depend on complex chemical and phase equilibria in downhole environments. Furthermore, the relationship between accelerated laboratory tests and the

Submitted for publication: March 3, 2015. Revised and accepted: June 27, 2015. Preprint available online: June 27, 2015, http://dx.doi.org/10.5006/1692. Presented in a preliminary form as paper 3744 at CORROSION 2014, March 9-13, 2014, San Antonio, Texas.

‡ Corresponding author. E-mail: aanderko@olisystems.com.
* OLI Systems Inc., 240 Cedar Knolls Road, Suite 301, Cedar Knolls, NJ 07927.
** DNV GL - Strategic Research and Innovation, 5777 Frantz Road, Dublin, OH 43017.

ISSN 0010-9312 (print), 1938-159X (online)
15/000195/$5.00+$0.50/0

actual field environment is often not quantified. Essentially, the performance of a given material needs to be understood in terms of its reliability in a given set of environmental conditions. Therefore, it is of interest to develop a predictive approach that covers a broad range of alloy-environment combinations using a limited set of experimental data coupled with a physical model that is capable of generalizing the experimental database and extrapolating from laboratory tests to field conditions.

From the point of view of CRAs in severe well environments, stress corrosion cracking (SCC) is of great interest because it can occur over wide ranges of conditions, including the moderate to high temperatures that are critical to downhole applications. For mapping the environmental ranges of SCC, it is crucial to identify a critical potential above which SCC can occur. SCC can be triggered if the corrosion potential of the metal (E_{corr}) exceeds the critical potential. It is generally recognized that localized corrosion can be a precursor to SCC. This principle has been established and extensively investigated in chloride environments by Tsujikawa and coworkers.[3-7] This is a result of the fact that the conditions that lead to localized corrosion (i.e., those that sustain a critical chemistry in an occluded environment inside a pit or crevice) are similar to the conditions that are needed to sustain SCC. The role of localized corrosion in the initiation of SCC has also been identified for sulfur-bearing environments, including those containing thiosulfates[8] and hydrogen sulfide.[9] In particular, experimental evidence exists that SCC in chloride-thiosulfate solutions occurs at potentials above the repassivation potential (E_{rp}) for localized corrosion, thus indicating that localized corrosion leads to the initiation of SCC.[8] Also, it has been shown through fracture mechanics testing that measurable crack growth occurs only at potentials more positive to E_{rp}.[8] This indicates that a reliable methodology for the prediction of SCC should be closely linked to the prediction of localized corrosion. Therefore, a project has been undertaken to:

1. Develop an electrochemical model for predicting the repassivation potential using a set of new E_{rp} measurements that capture the effects of key electrochemically active species such as Cl^- and H_2S;
2. Develop a model for predicting the corrosion potential of CRAs in oil and gas production environments; a combination of the E_{corr} and E_{rp} models will make it possible to predict the occurrence of localized corrosion;[10] and
3. Experimentally verify the hypothesis that the repassivation potential for localized corrosion is the appropriate critical potential above which SCC occurs. It should be noted that this is limited to the forms of environmentally assisted cracking for which localized corrosion is a precursor to cracking. Other forms of cracking such as sulfide stress cracking and hydrogen stress cracking occur according to different mechanisms and cannot be rationalized based on the approach described here. However, from the point of view of the performance of CRAs in severe oil and gas environments, SCC occurring at anodic potentials is of greater interest because it can occur over a wider range of environmental conditions, particularly at elevated temperatures.

This work focuses on part (1). Parts (2) and (3) will be the subject of separate studies.

To develop a model for predicting the repassivation potential in oil and gas environments, a previously developed model[11-12] for calculating E_{rp} in environments containing chlorides and various inhibitive oxyanions was extended. An especially useful feature of this model is its generalization in terms of the composition of Fe-Ni-Cr-Mo-W-N alloys,[13] which makes it possible to predict E_{rp} as a function of not only the environment chemistry but also the composition of the alloy. In particular, this generalization made it possible to predict the effect of chromium and molybdenum depletion on the repassivation potential of heat-treated alloys.[14-16] However, in its original form, the model is not applicable to systems containing H_2S or other aggressive sulfur species, thus making it necessary to develop a reformulated and extended version that incorporates the electrochemical effects of H_2S.

Various experimental studies have revealed that H_2S and, in general, adsorbed sulfur, have a strong effect on the mechanism of the dissolution of individual metals[17-26] and alloys.[27-28] This effect has a profound influence on the behavior of alloys in occluded environments associated with localized corrosion.[29-33] Moreover, alloy dissolution and localized corrosion are strongly affected by the formation of metal sulfides.[34-38] Insights from these studies are utilized in the present work to develop an electrochemical model for the repassivation potential of CRAs in environments containing Cl^- and H_2S.

In general, there is a very limited amount of experimental repassivation potential data in the literature.[9,39] Therefore, a comprehensive set of new E_{rp} data has been obtained in this study for a 13-Cr supermartensitic stainless steel (UNS S41425,[(1)] commonly referred to as S13Cr) to elucidate the interplay of Cl^- and H_2S in localized corrosion. These data cover a wide range of Cl^- and H_2S concentrations and were used to parameterize and verify the model. After verifying the model using the new E_{rp} measurements, the model was additionally tested using a limited amount of literature data.

[(1)] UNS numbers are listed in *Metals and Alloys in the Unified Numbering System*, published by the Society of Automotive Engineers (SAE International) and cosponsored by ASTM International.

EXPERIMENTAL PROCEDURES

Materials and Specimens

Specimens made out of Alloy S41425 supermartensitic stainless steel were used in the experiments. The chemical composition of this material is 12.10% Cr, 5.90% Ni, 1.90% Mo, 0.010% C, and balance Fe. Specimens in the form of a cylinder (for measurements on boldly exposed surfaces) and crevice samples were both used, with the dimensions shown in Figure 1. The crevice samples were prepared according to ASTM G192.[40] The sample surface was abraded with 600 grit SiC sandpaper, cleaned in an ultrasonic bath with isopropanol, and dried by blowing nitrogen. The creviced specimens were assembled using ceramic multiple-crevice formers wrapped with Teflon[†] tape. Bolts, nuts, and washers were made out of Ti alloy. Seventy in·lbf (7.91 N·m) torque was applied on the assembly to ensure the formation of critical crevice geometry.

Experimental Conditions

Electrochemical experiments were performed in NaCl solutions at various concentrations ranging from 3 molal to 0.0003 molal. All tests were performed at 85°C and ambient pressure. The experiments were conducted with and without the presence of H_2S. Premixed gases with different concentrations of H_2S in nitrogen were used to study the effect of H_2S. A multi-neck round-bottom flask described in ASTM G5[41] was used, which included a working electrode, a saturated calomel electrode (SCE) as the reference in a water-cooled Luggin probe, and a Pt/Nb loop as the counter electrode. The electrochemical cell held approximately 800 mL of solution in all tests. The Luggin probe was also filled with the test solution. In all of the tests, research-grade nitrogen was purged through the solution and testing cell while the entire setup was heated up to 85°C. Nitrogen sparging was maintained for at least 2.5 h to remove oxygen. Water vapor was collected by a condenser and flowed back into the cell. The sample was mounted on the electrode holder as described in ASTM G5.[41] The working electrode holder was quickly installed while maintaining nitrogen purging (with a positive pressure inside the glass cell). The sample was kept hanging over the solution surface in the nitrogen blanket for 10 min to 15 min to remove any introduced oxygen. Then, it was lowered and either partially immersed in the case of the cylindrical coupons (to avoid crevice corrosion for measurements on boldly exposed specimens) or fully immersed in the case of the crevice samples.

Electrochemical Experiments and E_{rp} Determination

After immersing the sample, the open circuit potential (OCP) of the specimen was monitored overnight while the solution was deaerated with nitrogen. In experiments with hydrogen sulfide, a H_2S gas mixture was introduced the next day and the solution was subsequently sparged with the gas mixture throughout the test. Electrochemical tests were started after OCP reached a steady state, which typically required 2 h. Following the OCP monitoring, dynamic potential scanning experiments were performed to obtain cyclic polarization curves. The dynamic potential scanning was started from –100 mV_{OCP} to 1 V_{SCE} or when the current density reached 1 mA/cm^2, whichever came first. The scanning rate was 0.167 mV/s.

In typical electrochemical experiments, the repassivation potential (E_{rp}) is selected as the crossover point of the reverse scan portion, with the forward scan portion on the polarization curve. In the present work, however, an inflection point often appeared on the reverse scan, indicating the change of passivation. When the anodic current density at the inflection point was within an order of magnitude of the passive current density in the forward scan, the potential at this point was selected to be the E_{rp}. Otherwise, E_{rp} was further confirmed by different electrochemical techniques, i.e., potentiostatic experiments without showing any localized attack for at least 24 h at a potential ~50 mV lower than the inflection point value, and the Tsujikawa-Hisamatsu Electrochemical (THE, also known as potentiodynamic-galvanostatic-potentiostatic) method[40] showing a current transition from increasing to decreasing at potentiostatic holding steps.

The measurements were performed on both creviced and boldly exposed samples. Following the

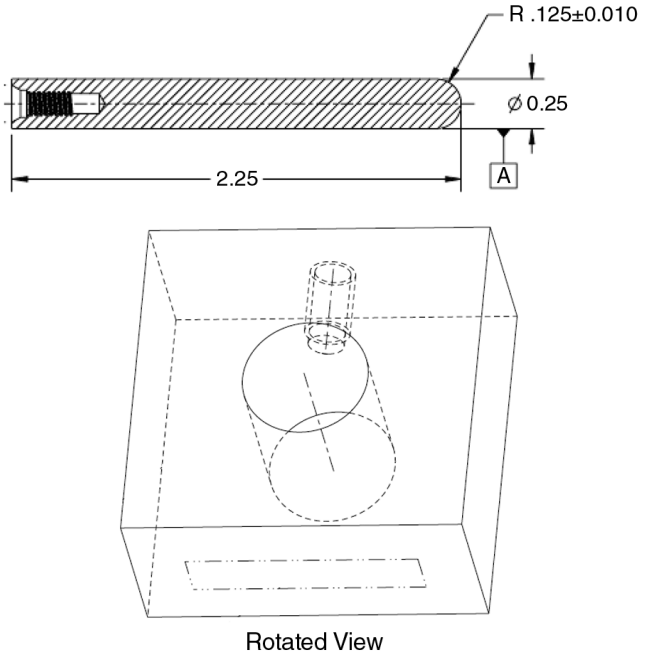

FIGURE 1. *Schematics of the specimens used in the electrochemical experiments for E_{rp} determination.*

[†] Trade name.

TABLE 1
Repassivation Potentials Measured for Alloy S41425 in Cl^--H_2S environments at 85°C[A]

NaCl Molal	a Cl^-[B]	wt% H_2S (gas phase)	Measurement Type[C]	E_{rp} (mV_{SCE})	E_{rp} (mV_{SHE})
0.0003	0.00029	0	C	45	199
0.0003	0.00029	0	C	29	183
0.003	0.0028	0	C	–104	49
0.003	0.0028	0	C	–120	33
0.03	0.025	0	C	–173	–22
0.3	0.203	0	C	–317	–168
0.3	0.203	0	C	–302	–153
3	2.01	0	B	–395	–249
3	2.01	0	B	–366	–220
0.0003	0.00029	1	C	260	414
0.003	0.0028	1	C	34	187
0.003	0.0028	1	C	–156	–3
0.003	0.0028	1	C	–255	–102
0.03	0.025	1	C	–210	–59
0.1	0.075	1	C	–356	–206
0.3	0.202	1	C	–391	–242
0.3	0.202	1	C	–441	–292
0.3	0.202	1	C	–434	–285
0.3	0.202	1	C	–341	–192
1	0.618	1	C	–437	–289
0.0003	0.00029	1	B	343	497
0.0003	0.00029	1	B	402	556
0.003	0.0028	1	B	85	238
0.03	0.025	1	B	24	175
0.03	0.025	1	B	–27	124
0.3	0.202	1	B	–156	–7
0.3	0.202	1	B	–151	–2
3	2.02	1	B	–433	–287
3	2.02	1	B	–449	–303
0.003	0.0028	100	C	–319	–166
0.03	0.025	100	C	–378	–227
0.0003	0.00029	100	B	–318	–164
0.0003	0.00029	100	B	–333	–179
0.003	0.0028	100	B	–325	–172
0.03	0.025	100	B	–356	–205
0.3	0.202	100	B	–548	–399
0.3	0.202	100	B	–542	–393
3	2.01	100	B	–593	–447
3	2.01	100	B	–588	–442

[A] The E_{rp} values are reported as directly measured with respect to an external SCE electrode and after conversion to the SHE scale (cf. the Appendix).
[B] Calculated from an electrolyte thermodynamic model[46] as implemented in OLI Studio†.[47]
[C] C: measurements with crevice samples, B: measurements with boldly exposed surfaces.

measurements, the tested specimens were removed from the solution and inspected under an optical microscope or a scanning electron microscope to confirm localized corrosion attack. Prior to the next cycle of measurements, the glass cell and accessories were soaked in 50% nitric acid to clean off corrosion products and subsequently cleaned with soap water, rinsed with deionized water, and dried.

The measured repassivation potentials are collected in Table 1. In order to be used for modeling, the

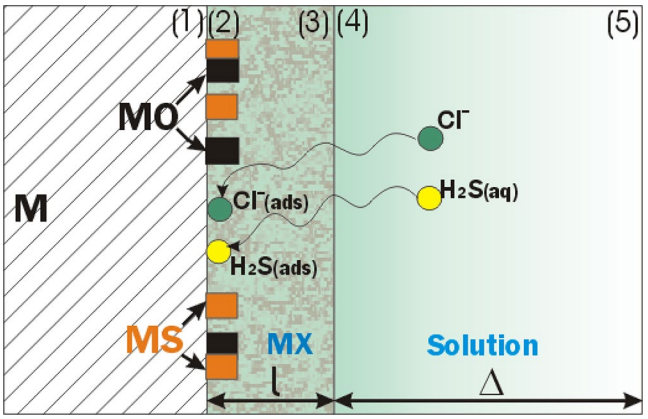

FIGURE 2. *Schematic summary of the phases and interfaces considered in the model (M: metal, MX: hydrous halide, MO: metal oxide, MS: metal sulfide).*

E_{rp} values have been converted to the standard hydrogen electrode (SHE) scale. This conversion includes a correction for the thermal junction potential and is described in detail in the Appendix. The Appendix also includes a table of corrections as a function of temperature and the NaCl concentration in the test solution. Table 1 lists both the E_{rp} values that were directly measured with respect to the external SCE electrode and those converted to the SHE scale using the procedure described in the Appendix.

COMPUTATIONAL MODEL

Repassivation Potential in Chloride Environments

The repassivation potential model for aqueous systems containing chlorides was described in detail in a previous study.[11] In this section, the fundamentals of this model are described to create a foundation for a more general model that accounts for the effects of H_2S.

Figure 2 schematically depicts the phases that are considered in an occluded localized corrosion environment. The metal M undergoes an anodic dissolution process below a layer of a nonprotective hydrous halide MX with a thickness of l. The hydrous halide further dissolves in a solution with a boundary layer thickness Δ. In general, the existence of a solid phase MX is not necessary as long as a solution phase with a halide concentration close to saturation is present at the metal interface. The process of repassivation entails the formation of a protective layer of metal oxide (MO), which is assumed to cover a certain fraction of the metal surface at a given time. The original E_{rp} model was derived[11] by considering the measurable potential drop across the interface as a sum of four contributions, i.e.,

$$E = \Delta\Phi_{M/MX}(1,2) + \Delta\Phi_{MX}(2,3) + \Delta\Phi_{MX/S}(3,4) + \Delta\Phi_{S}(4,5) \quad (1)$$

where the numbers in parentheses denote the interfaces shown in Figure 2: $\Delta\Phi_{M/MX}(1,2)$ is the potential difference at the metal/hydrous halide interface, $\Delta\Phi_{MX}(2,3)$ is the potential drop across the hydrous halide layer, $\Delta\Phi_{MX/S}(3,4)$ is the potential difference across the halide/solution interface, and $\Delta\Phi_S(4,5)$ is the potential drop across the solution boundary layer. The last three terms in Equation (1) can be evaluated in terms of fluxes and activities of metal and chloride ions using the methods of nonequilibrium thermodynamics introduced by Okada.[42] As derived previously,[11] the model is fully determined by the following equations:

i. An expression for the current density that results from metal dissolution across the (1,2) interface and is a function of $\Delta\Phi_{M/MX}(1,2)$, i.e.,

$$i = i\left(\Delta\Phi_{M/MX}(1,2)\right) \tag{2}$$

ii. An equation that relates the measurable potential, E, to the current density, i, and the activities of metal ions in the bulk solution (aM(5)) and at the metal interface (aM(2)), i.e.,

$$E = \Delta\Phi_{M/MX}(1,2) + \frac{Ki}{z_M^2F^2} + \frac{RT}{z_MF}\ln\frac{a_M(5)}{a_M(2)} \tag{3}$$

where K is a constant, z_M is the average metal charge, and R and F are the gas and Faraday constants, respectively; and

iii. A relationship between the activities of chloride ions or other solution species (a_j) and their fluxes in the hydrous halide (J_j') and the boundary layer (J_j''), i.e.,

$$\frac{RT}{z_jF}\ln\frac{a_j(5)}{a_j(2)} = \frac{Ki}{z_M^2F^2} + \frac{RT}{z_MF}\ln\frac{a_M(5)}{a_M(2)} - \frac{J_j'l}{z_jF\overline{n_j'}\overline{v_j'}} - \frac{J_j''\Delta}{z_jF\overline{C_j''}\overline{v_j''}} \tag{4}$$

where $\overline{n_j'}$ and $\overline{c_j''}$ are the average concentrations in the hydrous halide and the boundary layer, respectively, and $\overline{v_j'}$ and $\overline{v_j''}$ are the corresponding average mobilities in these phases.

Equations (3) and (4) can be simplified in the limit of repassivation when the current density reaches a certain small value, $i = i_{rp}$ (typically, $i_{rp} = 10^{-2}$ A/m^2) and, simultaneously, the fluxes of active species and metal ions become small and comparable to those resulting from passive dissolution. Then, it can be shown that in the limiting case of $E = E_{rp}$, Equations (3) and (4) simplify to:[11]

$$E_{rp} = \Delta\Phi_{M/MX}(1,2) + K_1 \tag{5}$$

$$\frac{a_j(5)}{a_j(2)} \approx K_2 \tag{6}$$

where K_1 and K_2 are constants. To obtain a working equation for E_{rp}, a detailed expression needs to be established for $i(\Delta\Phi_{M/MX}(1,2))$ (Equation [2]), which reflects the mechanism of active dissolution and oxide formation. Such an expression was developed in the previous study[11] for environments containing chlorides and inhibitive oxyanions. However, the previously established expression for $i(\Delta\Phi_{M/MX}(1,2))$ is not suitable for H_2S-containing systems because it does not take into account the electrochemical behavior of metal interfaces with an adsorbed sulfur layer.

An expression that satisfies this requirement will be derived in the next section. While a new expression for $i(\Delta\Phi_{M/MX}(1,2))$ is necessary for systems containing H_2S, Equations (1) through (6) still apply. For simplicity, the derivation will be limited to Cl^- and H_2S as electrochemically active species. An extension to multicomponent systems will be presented in a future study.

Repassivation Potential in Environments Containing Cl^- and H_2S

To extend the model to systems containing H_2S, competitive adsorption of H_2S, Cl^- ions, and water were considered. The coverage fractions of H_2S, Cl^-, and H_2O on a surface corroding in the active state are denoted by θ_s, θ_c, and θ_o, respectively. The reactions at the metal surface may further lead to the formation of a metal oxide (MO) and metal sulfide (MS). The surface coverage fractions of MO and MS are denoted by Ψ_{MO} and Ψ_{MS}, respectively. In systems that do not contain other electrochemically active species, the surface fractions satisfy the balance equation:

$$\theta_c + \theta_s + \theta_o + \Psi_{MO} + \Psi_{MS} = 1 \tag{7}$$

Adsorption of Cl^- ions can be considered as a replacement of H_2O on the metal surface (M) with Cl^-, i.e.,

$$\underset{\theta_o}{MH_2O_{ads}} + Cl^- \underset{r_c^{\leftarrow}}{\overset{r_c^{\rightarrow}}{\rightleftharpoons}} \underset{\theta_c}{MCl^-_{ads}} + H_2O \tag{8}$$

where $r_c^{\rightarrow}$ and $r_c^{\leftarrow}$ are the adsorption and desorption rate constants, respectively, and the adsorption coverage fractions θ_o and θ_c are placed below the adsorbed species to indicate the correspondence between the surface species and their coverage fractions. M is a metal whose properties are an appropriate average of those of the alloy components. In accordance with the previous studies,[11,13] the adsorption is followed by the dissolution of the adsorbed complex, i.e.,

$$\underset{\theta_c}{MCl^-_{ads}} \xrightarrow{i_c} M^{z+} + ze^- + Cl^- \tag{9}$$

where i_c is the c urrent density associated with the dissolution of the MCl^-_{ads} complex and z is the aver-

age charge. The process of repassivation is associated with the formation of a metal oxide layer according to the reaction:

$$\underset{\theta_o}{MH_2O_{ads}} + (z/2-1)H_2O \xrightarrow{i_{MO}} \underset{\Psi_{MO}}{MO_{z/2}} + zH^+ + ze^- \quad (10)$$

where i_{MO} is the cu rrent density that is associated with the formation of the oxide. It is important to consider the presence of adsorbed H_2O in Equations (8) and (10) because water is the necessary precursor for the formation of oxide.[42] The surface oxide $MO_{z/2}$ can be further dissolved through a chemical dissolution process, i.e.,

$$\underset{\Psi_{MO}}{MO_{z/2}} + zH^+ \xrightarrow{k_{MO}} M^{z+} + (z/2)H_2O \quad (11)$$

where k_{MO} is a chemical dissolution rate constant.

The presence of H_2S gives rise to electrochemical reactions that may lead to a very significant enhancement of the anodic dissolution process and may result in the formation of a sulfide phase. The mechanisms of the H_2S-induced acceleration of anodic dissolution were extensively studied in the literature for Fe,[17-18,20-21,23-24] Ni,[18-19,22,26] Cr,[25] and Fe-Ni-Cr-Mo alloys.[27-28] In this study, a simplified version of a previously proposed mechanism was adopted.[17,20,23,26] The mechanism needs to be simplified because, in view of the available data, it is not possible to separate the reactions of the individual alloy components and it is necessary to limit the number of parameters that can be numerically evaluated to characterize the mechanism. Lumping the alloy components together prevents taking into account the different dissolution tendencies of individual alloy components (i.e., Fe, Ni, Cr, and Mo). Also, it excludes the detailed chemical characterization of the solid phases that form in the process of repassivation. These phases are primarily chromium oxides, which may form in the absence or presence of H_2S, and nickel[34,37] and iron sulfides, which may result from reactions involving H_2S. The oxide and sulfide phases will be denoted by $MO_{z/2}$ and $MS_{z/2}$, respectively. While forgoing the detailed characterization of the behavior of alloy components, this approach makes it possible to characterize the repassivation process of the alloy with a minimum number of parameters. Although it is recognized that the individual alloy elements contribute differently to the formation of the oxide and sulfide phases, as well as to the dissolution in the active state, the overall electrochemical parameters are defined for the alloy rather than its components.

In accordance with the previous studies,[17,20,23,26] a key step in the H_2S-mediated dissolution is the adsorption of H_2S on the surface. The adsorption can be written as a displacement of hydration water on the metal surface by hydrogen sulfide:

$$\underset{\theta_o}{MH_2O_{ads}} + H_2S \underset{\overleftarrow{r_s}}{\overset{\overrightarrow{r_s}}{\rightleftharpoons}} \underset{\theta_s}{MHS^-_{ads}} + H^+ + H_2O \quad (12)$$

where $\overrightarrow{r_s}$ and $\overleftarrow{r_s}$ are the H_2S adsorption and desorption rate constants, respectively. The adsorption is followed by an electrochemical step:

$$MHS^-_{ads} \longrightarrow MHS^{(z-1)+}_{ads} + ze^- \quad (13)$$

Equation (13) can be then followed by a dissolution reaction, which is responsible for the acceleration of the anodic process, i.e.,

$$MHS^{(z-1)+}_{ads} + H^+ \longrightarrow M^{z+} + H_2S \quad (14)$$

or it can be followed by the formation of a solid metal sulfide phase:

$$MHS^{(z-1)+}_{ads} + (z/2-1)H_2S \longrightarrow MS_{z/2} + (z-1)H^+ \quad (15)$$

In Equation (15), it can be assumed in practice that the effective formula of the metal sulfide is MS because NiS and mixed Ni-Fe sulfides are the predominant sulfides that may form on Fe-Ni-Cr alloys in aqueous solutions.[34,37] By adding Equations (13) and (14), the following equation is obtained:

$$\underset{\theta_s}{MHS^-_{ads}} + H^+ \xrightarrow{i_s} M^{z+} + H_2S + ze^- \quad (16)$$

where i_s is the current density associated with the H_2S-induced acceleration of anodic dissolution. Further, by adding Equations (13) and (15), Equation (17) is obtained:

$$\underset{\theta_s}{MHS^-_{ads}} + (z/2-1)H_2S \xrightarrow{i_{MS}} \underset{\Psi_{MS}}{MS_{z/2}} + (z-1)H^+ + ze^- \quad (17)$$

where i_{MS} is the current density for the formation of the metal sulfide. Thus, the mechanism reflects the competitive formation of metal oxide (Equation [10]) and metal sulfide (Equation [17]). This is illustrated schematically in Figure 2 and is in agreement with the experiments of Marcus and Grimal,[35] who observed the formation of islands of chromium oxide and nickel sulfide on a surface. The sulfur islands were found to persist even in a passivated system.

The metal sulfide may undergo chemical dissolution according to the reactions:

$$\underset{\Psi_{MS}}{MS_{z/2}} + zH^+ \xrightarrow{k_{MS}} M^{z+} + (z/2)H_2S \quad (18)$$

$$\underset{\Psi_{MS}}{MS_{z/2}} + (2-z/2)H_2S \xrightarrow{u_{MS'}} M(HS)^{z-2}_2 + (2-z)H^+ \quad (19)$$

where the second reaction recognizes the possibility of formation of complex aqueous species such as $Fe(HS)_2^0$ or $Ni(HS)_2^0$, whose existence has been postulated in thermodynamic studies.[43]

After defining the reactions that may occur in the system in the process of repassivation, the change of coverage fractions with time can be related to the current densities and rate constants defined above. Based on Equations (8) and (9), the change of the Cl^- coverage fraction is:

$$\frac{\partial\theta_c}{\partial t} = \vec{r_c}\theta_o a_c(2) - \overleftarrow{r_c}\theta_c - c_c i_c \qquad (20)$$

where $a_c(2)$ is the activity of Cl^- at the metal surface and c_c is a constant. The first and second terms on the right-hand side of Equation (20) represent the physical adsorption and desorption according to Equation (8), whereas the last term reflects the electrochemical desorption as a result of Equation (9). The current density i_c is related to θ_c in accordance with Equation (9):

$$i_c = i_c^0\theta_c \qquad (21)$$

where the symbol i_c^0 is introduced to simplify further notation and is given by:

$$i_c^0 = d_c \exp\left[\frac{\alpha_c F\Delta\Phi_{M/MX}(1,2)}{RT}\right] \qquad (22)$$

where d_c is a pre-exponential factor. From Equations (10) and (11), the rate of formation of the oxide is given by:

$$\frac{\partial\Psi_{MO}}{\partial t} = c_{MO}i_{MO} - k_{MO}\Psi_{MO} \qquad (23)$$

where the first term on the right-hand side is a result of the electrochemical reaction of oxide formation (Equation [10]) and the second term is a result of the chemical dissolution of the oxide (Equation [11]). The coefficient c_{MO} relates the increase in the oxide coverage factor, Ψ_{MO}, to the current density that leads to the formation of the oxide (i_{MO}), and k_{MO} is the dissolution rate of the oxide. Both the c_{MO} and k_{MO} coefficients will be related in further derivation to parameters that can be determined from experimental data. The current density i_{MO} is related to θ_o according to Equation (10):

$$i_{MO} = i_{MO}^0\theta_0 \qquad (24)$$

where

$$i_{MO}^0 = d_{MO} \exp\left[\frac{\xi_{MO}F\Delta\Phi_{M/MX}(1,2)}{RT}\right] \qquad (25)$$

and d_{MO} is a pre-exponential factor. The change in the H_2S surface coverage fraction results analogously from Equations (12), (16), and (17):

$$\frac{\partial\theta_s}{\partial t} = \vec{r_s}\theta_o a_s(2) - \overleftarrow{r_s}\theta_s - c_{MS}i_{MS} - c_s i_s \qquad (26)$$

where $a_s(2)$ is the activity of H_2S at the metal surface and c_{MS} and c_s are constants. The first and second terms on the right-hand side of Equation (26) represent the physical adsorption and desorption (Equation [12]), the third term reflects the electrochemical Equation (17) that leads to the formation of the metal sulfide, and the fourth term corresponds with the electrochemical desorption resulting from Equation (16). The current density i_{MS}, which is responsible for the formation of the metal sulfide according to Equation (17), is given by:

$$i_{MS} = i_{MS}^0\theta_s \qquad (27)$$

where

$$i_{MS}^0 = d_{MS} \exp\left[\frac{\xi_{MS}F\Delta\Phi_{M/MX}(1,2)}{RT}\right] \qquad (28)$$

and the current density that accounts for H_2S-accelerated dissolution is:

$$i_s = i_s^0\theta_s \qquad (29)$$

where the factor i_s^0 is given by

$$i_s^0 = d_s \exp\left[\frac{\alpha_s F\Delta\Phi_{M/MX}(1,2)}{RT}\right] \qquad (30)$$

In Equations (26), (27), and (29), it is assumed that z = 2 in Equation (17). The rate of formation of the sulfide layer is expressed as:

$$\frac{\partial\Psi_{MS}}{\partial t} = c_{MS}i_{MS} - k_{MS}\Psi_{MS} - u_{MS}'a_s(2)\Psi_{MS} = c_{MS}i_{MS} - k_{MS}\Psi_{MS}(1 + u_{MS}a_s(2)) \qquad (31)$$

where the first term on the right-hand side of Equation (31) is a consequence of Equation (17) and the second and third terms result from the chemical dissolution of the sulfide, i.e., Equations (18) and (19), respectively. The coefficient c_{MS} relates the increase in the metal sulfide coverage factor, Y_{MS}, to the current density that leads to the formation of the sulfide, i_{MS}. The coefficients k_{MS} and u_{MS}' are the rate constants for the dissolution of the sulfide according to Equations (18) and (19), respectively.

The total anodic current density is a sum of those for the individual processes, i.e.,

$$i = i_c + i_{MO} + i_s + i_{MS} \qquad (32)$$

In the steady state, which corresponds to the limit of repassivation, the surface coverage fractions no longer undergo a change. Hence,

$$\frac{\partial\theta_c}{\partial t} = \frac{\partial\Psi_{MO}}{\partial t} = \frac{\partial\theta_s}{\partial t} = \frac{\partial\Psi_{MS}}{\partial t} = 0 \qquad (33)$$

The condition (33), together with Equations (20), (23), (26), and (31), gives four equations that depend on θ_c, θ_o, Ψ_{MO}, θ_s, and Ψ_{MS}. By substituting θ_o from the surface coverage balance Equation (7), the five variables θ_c, θ_o, Ψ_{MO}, θ_s, and Ψ_{MS} can be obtained analytically. Then, these variables are substituted into the defining equations for i_c, i_{MO}, i_{MS}, and i_s (Equations [21] and [22], [24] and [25], [27] and [28], and [29] and [30], respectively) and the resulting expressions for current densities are summed according to Equation (32). The resulting expression for the total current density is:

See Equation (34) at the Bottom of the Page (34)

Equation (34) can be solved in the limit of repassivation, i.e., when $E = E_{rp}$ and $i = i_{rp}$. For this purpose, Equations (5) and (6) are utilized, which are valid in the repassivation limit. Then, Equation (34) becomes:

See Equation (35) at the Bottom of the Page (35)

where $r_c = \vec{r_c}/(\overleftarrow{r_c}K_2)$ and $r_s = \vec{r_s}/(\overleftarrow{r_s}K_2)$ are rescaled adsorption equilibrium constants for Cl^- and H_2S, respectively, $a_c = a_c(5)$ and $a_s = a_s(5)$ are the activities of Cl^- and H_2S, respectively, in the bulk environment, and

$$e_c = c_c / \overleftarrow{r_c} \qquad (35a)$$

$$e_s = c_s / \overleftarrow{r_s} \qquad (35b)$$

$$e_{MS} = c_{MS} / \overleftarrow{r_c} \qquad (35c)$$

$$i_p = k_{MO} / c_{MO} \qquad (35d)$$

$$i_q = k_{MS} / c_{MS} \qquad (35e)$$

In the limit of repassivation, the expressions for i_c^0, i_{MO}^0, i_{MS}^0, and i_s^0 take the form:

$$i_c^0 = d_c \exp\left[\frac{\alpha_c F\left(E_{rp} - K_1\right)}{RT}\right] = f_c \exp\left[\frac{\alpha_c F E_{rp}}{RT}\right] \qquad (36)$$

$$i_{MO}^0 = d_{MO} \exp\left[\frac{\xi_{MO} F\left(E_{rp} - K_1\right)}{RT}\right] = f_{MO} \exp\left[\frac{\xi_{MO} F E_{rp}}{RT}\right] \qquad (37)$$

$$i_{MS}^0 = d_{MS} \exp\left[\frac{\xi_{MS} F\left(E_{rp} - K_1\right)}{RT}\right] = f_{MS} \exp\left[\frac{\xi_{MS} F E_{rp}}{RT}\right] \qquad (38)$$

$$i_s^0 = d_s \exp\left[\frac{\alpha_s F\left(E_{rp} - K_1\right)}{RT}\right] = f_s \exp\left[\frac{\alpha_s F E_{rp}}{RT}\right] \qquad (39)$$

where f_c, f_{MO}, f_{MS}, and f_s are rescaled pre-exponential factors, which incorporate the unknown value of K_1.

Equation (35), coupled with Equations (36) through (39), constitutes the fundamental equation for finding the value of E_{rp}. However, it needs to be simplified for a practical application of the model.

Practical Implementation of the Model

To make the model manageable with respect to the number of parameters, it was observed that the coefficients e_c (i.e., $e_c = c_c/\overleftarrow{r_c}$) and e_s (i.e., $e_s = c_s/\overleftarrow{r_s}$) could be neglected. This is because, at the low current densities at repassivation, the electrochemical desorption terms in Equations (20) and (26), which result from the existence of the current densities i_c and i_s, can be expected to be less significant than the physical desorption terms. Thus, the coefficients c_c and c_s can be expected to be much smaller than the desorption rate constants $\overleftarrow{r_c}$ and $\overleftarrow{r_s}$ in Equations (20) and (26). Also, preliminary numerical tests have revealed that the terms that contain the e_c and e_s coefficients can be neglected in Equation (35). On the other hand, the coefficient e_{MS} (Equation [35c]) cannot be neglected, although it can be expected to be small. Then, Equation (35) reduces to:

$$i_{rp} = \frac{\left(i_c^0 r_c a_c + i_{MO}^0\right)\left(1 + e_{MS} i_{MS}^0\right) + \left(i_{MS}^0 + i_s^0\right) r_s a_s}{\left[1 + r_c a_c + \frac{i_{MO}^0}{i_p}\right]\left(1 + e_{MS} i_{MS}^0\right) + r_s a_s \left(1 + \frac{i_{MS}^0}{i_q\left(1 + u_{MS} a_s\right)}\right)} \qquad (40)$$

$$i = \frac{\left[i_c^0 \frac{\vec{r_c} a_c(2)}{\overleftarrow{r_c}} + i_{MO}^0\left(1 + \frac{c_c i_c^0}{\overleftarrow{r_c}}\right)\right]\left(1 + \frac{c_{MS} i_{MS}^0}{\overleftarrow{r_s}} + \frac{c_s i_s^0}{\overleftarrow{r_s}}\right) + \left(i_{MS}^0 + i_s^0\right)\frac{\vec{r_s} a_s(2)}{\overleftarrow{r_s}}\left(1 + \frac{c_c i_c^0}{\overleftarrow{r_c}}\right)}{\left[1 + \frac{c_c i_c^0}{\overleftarrow{r_c}} + \frac{\vec{r_c} a_c(2)}{\overleftarrow{r_c}} + \frac{c_{MO} i_{MO}^0}{k_{MO}}\left(1 + \frac{c_c i_c^0}{\overleftarrow{r_c}}\right)\right]\left(1 + \frac{c_{MS} i_{MS}^0}{\overleftarrow{r_s}} + \frac{c_s i_s^0}{\overleftarrow{r_s}}\right) + \frac{\vec{r_s} a_s(2)}{\overleftarrow{r_s}}\left(1 + \frac{c_c i_c^0}{\overleftarrow{r_c}}\right)\left(1 + \frac{c_{MS} i_{MS}^0}{k_{MS}\left(1 + u_{MS}\, a_s(2)\right)}\right)}$$

Equation (34)

$$i_{rp} = \frac{\left[i_c^0 r_c a_c + i_{MO}^0\left(1 + e_c i_c^0\right)\right]\left(1 + e_{MS} i_{MS}^0 + e_s i_s^0\right) + \left(i_{MS}^0 + i_s^0\right) r_s a_s \left(1 + e_c i_c^0\right)}{\left[1 + e_c i_c^0 + r_c a_c + \frac{i_{MO}^0}{i_p}\left(1 + e_c i_c^0\right)\right]\left(1 + e_{MS} i_{MS}^0 + e_s i_s^0\right) + r_s a_s \left(1 + e_c i_c^0\right)\left(1 + \frac{i_{MS}^0}{i_q\left(1 + u_{MS} a_s\right)}\right)}$$

Equation (35)

The repassivation potential is then obtained numerically by solving a single nonlinear equation with respect to E_{rp}, i.e., Equation (40) with i_c, i_{MO}, i_{MS}, and i_s defined by Equations (36) through (39). Following previous work,[11,13] the activities a_c and a_s are calculated from an electrolyte thermodynamic model.[44-47] The thermodynamic model provides the activities of all aqueous species that are in equilibrium with an H_2S-containing gas phase. At the conditions investigated here, H_2S exists in the aqueous phase predominantly in the form of a neutral species $H_2S_{(aq)}$ and, therefore, there is no need to include other sulfur-bearing species in the E_{rp} model.

As in the previous study,[11] it is convenient to express the rate constants f_j (j = c, MO, MS, or s) in Equations (36) through (39) using corresponding Gibbs energies of activation, i.e.,

$$f_j = \exp\left(-\frac{\Delta g_j^{\neq}}{RT}\right) \quad (41)$$

where j = c, MO, s, or MS. An analogous equation expresses the dissolution rate constant u_{MS} in terms of the corresponding Gibbs energy of activation, $\Delta g_{dis,MS}^{\neq}$, i.e.,

$$u_{MS} = \exp\left(-\frac{\Delta g_{dis,MS}^{\neq}}{RT}\right) \quad (42)$$

The Gibbs energy of activation may be temperature-dependent according to the relation:

$$\frac{\Delta g_j^{\neq}}{RT} = \frac{\Delta g_j^{\neq}(T_{ref})}{RT} + \Delta h_j^{\neq}\left(\frac{1}{T} - \frac{1}{T_{ref}}\right) \quad (43)$$

where T_{ref} is a reference temperature (T_{ref} = 298.15 K). The adsorption equilibrium constants are expressed using the Gibbs energy of adsorption, i.e.,

$$r_j = \exp\left(-\frac{\Delta g_{ads,j}}{RT}\right) \quad (44)$$

where j = c and s. For the coefficient f_s in Equation (39), a first-order dependence on the activity of chlorides is assumed, i.e.,

$$f_s = f_s' a_c \quad (45)$$

where f_s' is expressed by Equations (41) and (43). This reflects the synergistic effect of H_2S and Cl^- on anodic dissolution. The remaining coefficients f_j (j = c, MO, and MS) depend only on temperature according to Equations (41) and (43). For simplicity, the electrochemical transfer coefficients in Equations (36) and (39) are assumed to be 1, i.e.,

$$\alpha_c = \alpha_s = 1 \quad (46)$$

On the other hand, the electrochemical transfer coefficient ξ_{MO} in Equation (37) needs to have a value that is lower than 1, which is necessary for accurately determining the slope of E_{rp} versus chloride concentration in the low-chloride, high-slope region.[11,13] The coefficient ξ_{MO} can be assigned the same value for various alloys as determined previously.[13] The electrochemical transfer coefficient for metal sulfide formation, ξ_{MS}, can be assumed to be the same as that for oxide formation, i.e.,

$$\xi_{MO} = \xi_{MS} \quad (47)$$

The constants i_p and i_q in Equation (40) are assigned the value 10^{-4} A/m^2. This results from the fact that i_p is equal to the passive current density,[11] for which 10^{-4} A/m^2 is a reasonable approximation for CRAs. The constant i_q, which is an analog of i_p for a metal surface covered with the sulfide rather than the oxide (cf. Equations [35d] and [35e]), can be expected to have a comparable value and is also assumed to be equal to 10^{-4} A/m^2.

RESULTS AND DISCUSSION

First, the model has been applied to Alloy S41425 in chloride-only environments because such environments provide a baseline for analyzing the effect of H_2S. In addition to the new E_{rp} data reported in Table 1, a substantial number of experimental measurements is available from a previous study[13] for Alloy S41425 in Cl^- solutions at 23°C, 60°C, and 95°C. In Cl^- systems, the model is completely defined when six parameters are specified: the Gibbs energy $\Delta g_c^{\neq}(T_{ref})$ and enthalpy $\Delta h_c^{\neq}$ of activation for the anodic dissolution mediated by the adsorption of Cl^- ions (Equations [36], [41], and [43]), the Gibbs energy $\Delta g_{MO}^{\neq}(T_{ref})$ and enthalpy $\Delta h_{MO}^{\neq}$ of activation for the formation of the oxide (Equations [37], [41], and [43]), the electrochemical transfer coefficient for the formation of the oxide ξ_{MO} (Equation [37]), and the Gibbs energy of adsorption of Cl^- ions $\Delta g_{ads,c}$ (Equation [44]). These parameters have been determined as follows:

i. The parameters ξ_{MO} and $\Delta g_{ads,c}$ have been assigned their generalized values, which have been established in a previous study[13] on the basis of experimental data for 13 stainless steels and Ni-based alloys.
ii. The remaining four parameters (i.e., $\Delta g_c^{\neq}(T_{ref})$, $\Delta h_c^{\neq}$, $\Delta g_{MO}^{\neq}(T_{ref})$, and $\Delta h_{MO}^{\neq}$) have been determined by simultaneously regressing the combined experimental E_{rp} data from this study (Table 1 for 0% H_2S) and from a previous study.[13] In principle, these parameters could also be calculated from the generalized correlation,[13] but determining them directly from the experimental data for Alloy S41425 maximizes the accuracy of the model.

TABLE 2

Parameters of the Repassivation Potential Model and Their Values for Cl^- H_2S Systems

Model Parameter	Parameter Definition	Alloy	
		S41425	J91574
$\Delta g_c^{\neq}(T_{ref})$	Gibbs energy of activation for dissolution mediated by adsorption of Cl^- at reference T	–10.58	–12.9
$\Delta h_c^{\neq}$	Enthalpy of activation for dissolution mediated by adsorption of Cl^-	0.011	0.004
$\Delta g_{ads,c}$	Gibbs energy of adsorption of Cl^-	10	10
$\Delta g_{MO}^{\neq}(T_{ref})$	Gibbs energy of activation for oxide formation at reference temperature	24.24	26.7
$\Delta h_{MO}^{\neq}$	Enthalpy of activation for oxide formation	–0.005	0.003
$\xi_{MO} = \xi_{MS}$	Electrochemical transfer coefficients for oxide and sulfide formation	0.8	0.8
$\Delta g_s^{\neq}(T_{ref})$	Gibbs energy of activation for dissolution mediated by adsorption of H_2S at reference T	–21.05	Assumed
$\Delta g_{ads,s}$	Gibbs energy of adsorption of H_2S	–16.07	the same
$\Delta g_{MS}^{\neq}(T_{ref})$	Gibbs energy of activation for sulfide formation at reference T	0.40	as for
e_{MS}	Coupling parameter (c_{MS}/r_c^{*-})	0.001	S41425
$\Delta g_{dis,MS}^{\neq}$	Gibbs energy of activation for sulfide dissolution	–21.4	

iii. Among the regressed parameters, $\Delta g_c^{\neq}(T_{ref})$ and $\Delta h_c^{\neq}$ determine the Gibbs energy of activation for Cl^--mediated alloy dissolution as a function of temperature according to Equation (43). These parameters primarily influence the E_{rp} vs. Cl^- dependence at higher Cl^- concentrations, i.e., for Cl^- molalities above approximately 0.003. This corresponds to the low-slope segment of the E_{rp} vs. Cl^- curves. On the other hand, the parameters $\Delta g_{MO}^{\neq}(T_{ref})$ and $\Delta h_{MO}^{\neq}$ determine the E_{rp} values at lower Cl^- concentrations, at which the E_{rp} vs. Cl^- curves show a higher slope, as demonstrated in previous studies.[11,13] The fact that the low-slope and high-slope sections of the E_{rp} vs. Cl^- curves are sensitive to different parameters facilitates the determination of the parameters.

The model parameters are listed in Table 2. With these parameters, the model can accurately reproduce the experimental E_{rp} data as a function of chloride concentration and temperature. This is illustrated in Figure 3, which compares the calculated results with the data. It should be noted that it is convenient to plot E_{rp} as a function of chloride activity rather than concentration because the model is expressed in terms of activities and, most importantly, various chloride-containing solutions (not necessarily only binary NaCl solutions) can be uniformly characterized using the chloride activity. Thus, the E_{rp} vs. Cl^- activity plot has a more general character than a plot against Cl^- concentration.

As shown in Figure 3, the E_{rp} vs. chloride activity plot shows a typical pattern of a lower slope at higher Cl^- concentrations and a higher slope at lower concentrations. The temperature dependence of E_{rp} is strong only at low chloride concentrations and diminishes at high concentrations.

It should be noted that the model described here represents an improvement over the original version of the model,[11,13] even in the absence of H_2S. In the original version, a simplifying assumption was

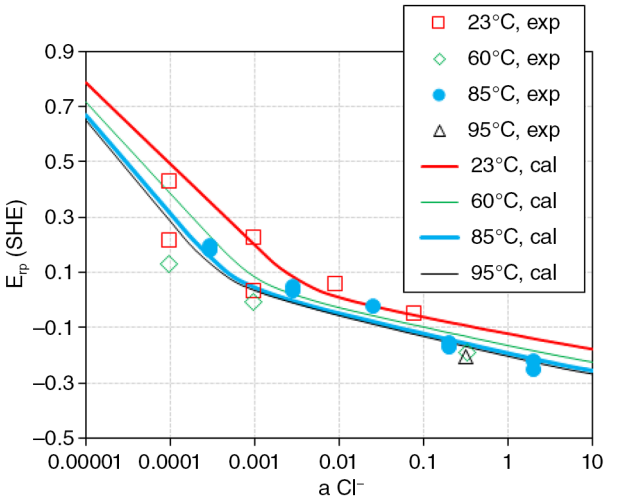

FIGURE 3. *Repassivation potential of Alloy S41425 in chloride solutions as a function of Cl^- activity at various temperatures. The symbols are the measurements from a previous study[13] (for 23, 60, and 95°C) and Table 1 (for 85°C) and the lines have been obtained from the model.*

made that the water coverage fraction θ_o was always equal to one, which was reasonable if the adsorption of all other species was fairly weak. Also, an empirical reaction order with respect to chloride ions was introduced, which was greater than 1. In the present model, the coverage fractions of all species including H_2O are rigorously interrelated (cf. Equation [7]) and there is no need to introduce empirical fractional reaction orders. Consequently, the reaction order with respect to Cl^- and other electrochemically active species is equal to 1 (cf. Equation [21]) and the parameterization of the model is simplified without a loss in accuracy.

After establishing the model for chloride-only systems, parameters have been determined for mixed Cl^--H_2S systems. These parameters include the Gibbs energy of adsorption of H_2S ($\Delta g_{ads,s}$), the Gibbs energies of activation for H_2S-accelerated dissolution, metal

sulfide formation, and sulfide chemical dissolution ($\Delta g^{\neq}_{s}(T_{ref})$, $\Delta g^{\neq}_{MS}(T_{ref})$, and $\Delta g^{\neq}_{dis,MS}$, respectively), and the parameter e_{MS}, which couples the sulfide formation with the desorption constant ($e_{MS} = c_{MS}/r_c^{-}$). The H_2S-related parameters have been determined as follows:

iv. The enthalpies of activation for H_2S-accelerated dissolution and metal sulfide formation (i.e., $\Delta h^{\neq}_{s}$ and $\Delta h^{\neq}_{MS}$ in Equation [43]) have been assumed to be zero for simplicity. These two parameters determine the temperature dependence of the H_2S-related phenomena, and will be investigated in future studies on the basis of experimental data measured over a wide range of temperatures.

v. The parameters $\Delta g_{ads,s}$ and $\Delta g^{\neq}_{s}(T_{ref})$ have been determined from the E_{rp} data at high Cl^- concentrations, at which the accelerating effect of H_2S on anodic dissolution is well established. The Gibbs energy of adsorption $\Delta g_{ads,s}$ determines the strength of adsorption and, therefore, influences by how much the H_2S effect differs for different H_2S concentrations at high Cl^- concentrations. The obtained value of $\Delta g_{ads,s}$ is more negative than the Gibbs energy of adsorption of Cl^- (i.e., $\Delta g_{ads,c}$), which indicates that the adsorption of H_2S is, as expected, stronger than that of Cl^-. The decrease in E_{rp} in the presence of H_2S is determined by the value of $\Delta g^{\neq}_{s}(T_{ref})$.

vi. The parameters $\Delta g^{\neq}_{MS}(T_{ref})$ and $\Delta g^{\neq}_{dis,MS}$ reflect the effect of metal sulfide formation on E_{rp}. Therefore, they have been determined based on the E_{rp} data at low Cl^- concentrations and 1% H_2S, at which the metal sulfide formation manifests itself in an increase in the repassivation potential (see further discussion later). The elevation of the E_{rp} beyond the baseline that would exist in the absence of metal sulfide formation is controlled by the $\Delta g^{\neq}_{MS}(T_{ref})$ value. The parameter $\Delta g^{\neq}_{dis,MS}$ reflects how readily the metal sulfide dissolves and, hence, it influences the threshold concentrations at which the effect of the metal sulfide appears.

vii. Finally, the parameter e_{MS} has been set equal to 10^{-3}. This parameter dampens the metal sulfide-induced elevation of E_{rp} at low chloride concentrations. An accurate determination of this parameter is not possible with the currently available data and, therefore, an approximate low value needs to be assumed. Numerical testing revealed that the results are not sensitive to this parameters as long as it remains of the order of 10^{-3}.

The obtained parameters are included in Table 2. In the analysis of E_{rp} data, preference has been given to measurements obtained on creviced samples whenever data obtained on creviced and boldly exposed samples were not in quantitative agreement.

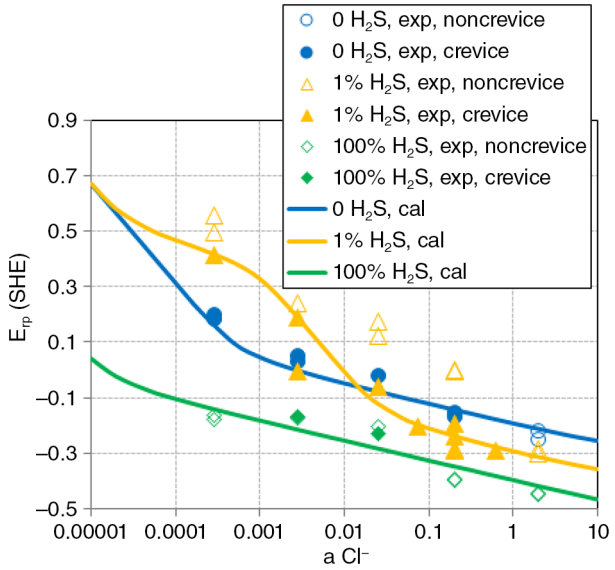

FIGURE 4. *Repassivation potential of Alloy S41425 at 85°C in Cl^- + H_2S systems as a function of Cl^- activity at three concentrations of H_2S in the gas phase (0, 1, and 100 wt%). The lines have been obtained from the model.*

In general, measurements on creviced samples give more reproducible results at less aggressive conditions when the alloy is less prone to localized corrosion. The differences between the measurements on creviced and boldly exposed samples are significant only at 1% H_2S and lower chloride concentrations (cf. Table 1). In more aggressive environments, the results obtained on both kinds of samples are quantitatively consistent.

The results of calculations are shown in Figure 4 in comparison with those for H_2S-free environments at 358.15 K. Figure 4 indicates that the effect of H_2S on the repassivation potential is very complex. At high H_2S concentrations (100 wt%), the E_{rp} vs. Cl^- curve is almost parallel to that in the absence of H_2S, but is shifted toward lower potentials by approximately 0.2 V. This is a manifestation of the acceleration of anodic dissolution in the localized environment by the presence of H_2S. As a result, H_2S strongly increases the tendency of the alloy to undergo localized corrosion at Cl^- concentrations ranging from 0.0003 m to 3 m provided that the H_2S concentration is sufficiently high (cf. the lowest line and the diamond symbols in Figure 4). On the other hand, the effect of H_2S at lower H_2S concentrations (i.e., 1 wt%) strongly depends on the chloride concentration. At high chloride concentrations, the behavior of the alloy in environments with 1% and 100% H_2S is similar, with the E_{rp} depression in 1% H_2S being, as expected, weaker. This results from the fact that the adsorption of H_2S is strong[48-50] and, therefore, 1% H_2S in the gas phase is sufficient to obtain a substantial H_2S coverage on the metal surface. Thus, as long as the mechanism of H_2S-accelerated anodic dissolution remains the same

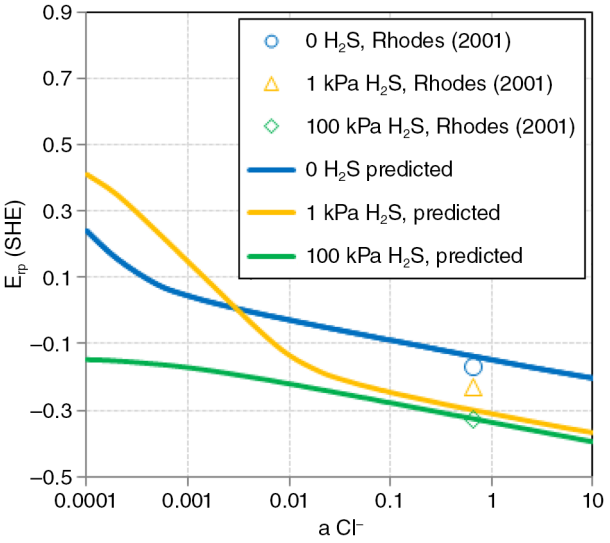

FIGURE 5. *Comparison of predicted repassivation potentials of Alloy J91574 with the experimental data of Rhodes[9] for Cl^- + H_2S systems at 25°C.*

(which appears to be the case at high chloride concentrations), the difference between the E_{rp} values at 1% and 100% H_2S is not large.

However, a drastically different behavior is observed at low chloride concentrations, which indicates a change in mechanism. In the low-Cl^- range, there is no reduction in E_{rp} because of H_2S and, instead, E_{rp} increases even above its level in Cl^--only solutions. It should be noted that this phenomenon was previously observed by Hinds, et al.,[27] in environments with low H_2S concentrations in the gas phase. This effect is a result of the formation of solid metal sulfide in competition with metal oxide. The presence of metal sulfide has a strong inhibitive effect. The net behavior of the system is a result of the competition between the acceleration of anodic dissolution from the adsorption of H_2S and the inhibition from the formation of a solid sulfide phase. At chloride activities below approximately 0.03, the effect of metal sulfide formation is predominant and leads to an increase in the repassivation potential by as much as 200 mV. Thus, under such low-H_2S and low-Cl^- conditions, H_2S effectively inhibits localized corrosion. The transition between the enhancement and inhibition of localized corrosion is predicted to occur over a narrow range of Cl^- activities (between approximately 0.01 and 0.05), which is in agreement with the experimental data. Thus, the model correctly represents the complex dependence of E_{rp} on both Cl^- and H_2S concentration.

At very low chloride concentrations, the E_{rp} lines for 0% H_2S and 1% H_2S converge (c.f., Figure 4). In this region, the potential becomes too high for the metal sulfides to persist. At such potentials, metal sulfides should not be stable because they should oxidize to higher oxidation states of sulfur.[51] Also, Marcus and Protopopoff[48-49] showed a similar limit of the stability field of adsorbed sulfur at higher potentials. Because the E_{rp} enhancement is attributed to the effect of metal sulfides, it should disappear at high potentials.

While the results of calculations for Alloy S41425 prove that the model can accurately reproduce the repassivation potential as a function of Cl^- and H_2S, they do not prove by themselves that the model has a predictive character. To verify whether the model is truly predictive, it is necessary to apply it to other metals and/or other conditions. Such calculations are shown in Figure 5 for Alloy CA6NM (UNS J91574) and compared with the approximate E_{rp} data of Rhodes.[9] The data of Rhodes[9] were obtained at 298 K, which is 60 K lower than the temperature used for the measurements reported here. For Alloy J91574 in H_2S-free environments, the model parameters have been calculated on the basis of the predictions from the previously developed generalized correlation.[13] The parameters that reflect the effect of H_2S have been simply assumed to be the same as those for Alloy S41425 (cf. Table 2). Thus, the model was used in a purely predictive manner for Alloy J91574, i.e., no parameters were adjusted based on the data that are specific to this alloy. As shown in Figure 5, the predicted results are in a good agreement with the data. Additionally, these results indicate that the H_2S effect on E_{rp} is not appreciably influenced by temperature, at least in the 298 K to 358 K range.

To verify the model further, it is necessary to analyze the behavior of additional alloys, especially those that are more corrosion-resistant than Alloy S41425. Experimental and modeling work is currently in progress for selected nickel-based and duplex alloys and will be reported in a forthcoming study.

It is of interest to compare the effect of H_2S on localized corrosion with the effect of thiosulfate ions, which was investigated by Newman, Garner, Laycock, and coworkers.[29-33] A considerable similarity exists between the effects of H_2S and thiosulfate because thiosulfate ions lead to substantial acceleration of dissolution. As with the H_2S-accelerated anodic dissolution mechanism proposed in this study, thiosulfate was demonstrated to activate anodic dissolution on the bare metal surface through the formation of a layer of adsorbed sulfur, which resulted from the electroreduction of the thiosulfate ion. However, the effect of thiosulfate appears to have its own complexity because inhibition of localized corrosion was found for increasing concentrations of thiosulfate, beyond a certain concentration. In view of the potential use of thiosulfate-containing systems as an alternative model environment for studying corrosion in sour environments, Tsujikawa, et al.,[52] found that the concentration of H_2S in thiosulfate-containing acidic solutions decreased with time and none was found in 316L stainless steel (UNS S31603) unless it was scratched. It has been speculated that H_2S was created from

thiosulfate through the disproportionation reaction to elemental sulfur, which was then either chemically or electrochemically reduced to H_2S.[52] While it is possible that such reactions may occur in active pits, it appears that the effect of thiosulfate is much more complex than that of H_2S. Therefore, it was not considered viable to attempt a unified treatment of localized corrosion in H_2S and thiosulfate environments in the current state of knowledge, and the methodology presented in this study is limited to H_2S systems.

Finally, it is of interest to highlight the commonalities and differences of the present model and the reactive transport models that are available in the literature. A pioneering reactive transport model was developed by Galvele[53-54] and extensively used to elucidate the pitting and, secondarily, repassivation potentials (cf. a review by Newman[55]). In common with the model presented here, the Galvele model relates the potential drop within the occluded space to the current density and the concentrations of various species (cf. Equation [1]). Therefore, some experimental observations can be explained by both models (in particular, the linear dependence of E_{rp} on chloride activity at higher chloride concentrations). In Galvele's model, it is assumed that the main triggering mechanism for pitting is the acidification of the pit and the attainment of a critical pH for depassivation. Further, the role of aggressive species such as chloride is mainly to affect the transport processes (and hence the conductivity) and, secondarily, the activity of protons (which is included qualitatively through a correction factor). Indeed, a key conclusion of the Galvele model is that the effect of aggressive species on pitting and protection potentials can all be accounted for through their effect on the transport processes. However, a correction factor is added for inhibiting species, which is not related to transport. Although the Galvele model laid an important milestone for thinking about localized corrosion, it has significant limitations in explaining experimental observations related to the effects of chloride and H_2S. First, the fundamental assumption about the central role of transport cannot explain the double slope that is observed for the repassivation potential vs. chloride concentration. Therefore, other surface reactions (namely the effect of water on passivation) have to be invoked and are essential at low chloride concentrations.[11] In the present model, the effect of chloride activity appears explicitly in the working equation that is solved for E_{rp} (i.e., Equation [40]) and is a consequence of the contribution to the current density as a result of the adsorption of Cl^- ions (cf. Equations [20] and [21]). At low chloride concentrations, the slope of the E_{rp} vs. Cl^- curve changes because of the additional contribution to the current density resulting from the oxide formation (cf. Equations [23] and [24]). Most importantly, in acidic H_2S solutions, the predominant species is the neutral H_2S molecule which will not affect conductivity through electromigration. Therefore, the role of H_2S in repassivation potential cannot be easily explained by Galvele's model. Instead, the complex effect of H_2S is explained in the present model through interfacial reactions that lead either to the acceleration of anodic dissolution or its inhibition via metal sulfide formation. At the limit of repassivation, the surface reactions that occur at the pit bottom play a central role in the present model, whereas the transport processes, while important in general, play a subsidiary role because the current density is low in the limit of repassivation.

CONCLUSIONS

- A systematic study has been undertaken to provide the values of the repassivation potential of corrosion-resistant alloys as a criterion for predicting whether the alloys can undergo localized corrosion and stress corrosion cracking in oil and gas-related environments.
- A comprehensive set of E_{rp} data has been obtained for Alloy S41425 in Cl^- + H_2S environments at 358.15 K.
- A model for calculating the repassivation potential as a function of solution chemistry and temperature has been developed. The model considers competitive adsorption, enhancement of anodic dissolution resulting from the adsorption of electrochemically active species, and competitive formation of metal oxide and sulfide in the process of repassivation.
- The presence of H_2S can substantially reduce the repassivation potential, thus indicating a strongly enhanced tendency for localized corrosion and SCC. However, exceptions exist at lower H_2S and Cl^- concentrations, at which H_2S may lead to the inhibition of localized corrosion. This complex behavior is accurately represented by the model.

ACKNOWLEDGMENTS

The work reported here was supported by Chevron, ConocoPhillips, DNV GL, JFE, Nippon Steel & Sumitomo Metal, Petrobras, Sandvik, and Vallourec-Manesmann within the framework of the joint industry program "Performance Assessment of CRAs in Severe Well Environments."

REFERENCES

1. NACE TM0177-2005, "Laboratory Testing of Metals for Resistance to Sulfide Stress Cracking and Stress Corrosion Cracking in H_2S Environments" (Houston, TX: NACE International, 2005).
2. NACE MR0175/ISO 15156-2, "Petroleum and Natural Gas Industries—Materials for Use in H_2S-Containing Environments in Oil and Gas Production" (Houston, TX: NACE, 2009).
3. S. Tsujikawa Y. Hisamatsu, *J. Japan Inst. Met.* 41, 8 (1977): p. 829-837.
4. T. Shinohara, S. Tsujikawa, Y. Hisamatsu, *Boshoku Gijutsu* 34, 5 (1985): p. 283-290.
5. T. Sugishita, T. Shinohara, S. Tsujikawa, Y. Hisamatsu, *Boshoku Gijutsu* 36, 12 (1987): p. 697-701.

6. T. Shinohara, Y. Atarashiya, S. Tsujikawa, *Corros. Eng.* 46, 11 (1997): p. 695-701.
7. S. Tsujikawa, *Corros. Eng.* 47, 1 (1998): p. 2-14.
8. G.A. Cragnolino, D.S. Dunn, Y.-M. Pan, N. Sridhar, "The Critical Potential for the Stress Corrosion Cracking of Fe-Ni-Cr Alloys and Its Mechanistic Implications," in *Chemistry and Electrochemistry of Corrosion and Stress Corrosion Cracking: A Symposium Honoring the Contributions of R.W. Staehle*, ed. R.H. Jones (Warrendale, PA: TMS, 2001), p. 83-104.
9. P.R. Rhodes, *Corrosion* 57, 11 (2001): p. 923-966.
10. N. Sridhar, C.S. Brossia, D.S. Dunn, A. Anderko, *Corrosion* 60, 10 (2004): p. 915-936.
11. A. Anderko, N. Sridhar, D.S. Dunn, *Corros. Sci.* 46, 7 (2004): p. 1583-1612.
12. A. Anderko, N. Sridhar, L.T. Yang, S.L. Grise, B.J. Saldanha, M.H. Dorsey, *Corros. Eng. Sci. Technol.* 40, 1 (2005): p. 33-42.
13. A. Anderko, N. Sridhar, M.A. Jakab, G. Tormoen, *Corros. Sci.* 50, 12 (2008): p. 3629-3647.
14. A. Anderko, N. Sridhar, G. Tormoen, *Corros. Eng. Sci. Technol.* 45, 3 (2010): p. 204-223.
15. N. Sridhar, G. Tormoen, S. Hackney, A. Anderko, *Corrosion* 65, 10 (2009): p. 650-662.
16. G. Tormoen, N. Sridhar, A. Anderko, *Corros. Eng. Sci. Technol.* 45, 2 (2010): p. 155-162.
17. Z.A. Iofa, V.V. Batrakov, Cho-Ngok-Ba, *Electrochim. Acta* 9 (1964): p. 1645-1653.
18. P. Süry, *Corros. Sci.* 16 (1976): p. 879-901.
19. J. Oudar, P. Marcus, *Appl. Surf. Sci.* 3 (1979): p. 48-67.
20. D.W. Shoesmith, P. Taylor, M.G. Bailey, D.G. Owen, *J. Electrochem. Soc.* 127, 5 (1980): p. 1007-1015.
21. D.R. Morris, L.P. Sampaleanu, D.N. Veysey, *J. Electrochem. Soc.* 127, 6 (1980): p. 1228-1235.
22. S. Ando, T. Suzuki, K. Itaya, *J. Electroanal. Chem.* 412, (1996): p. 139-146.
23. H.Y. Ma, X.L. Cheng, S.H. Chen, C. Wang, J.P. Zhang, H.Q. Yang, *J. Electroanal. Chem.* 451 (1998): p. 11-17.
24. X.L. Cheng, H.Y. Ma, J.P. Zhang, X. Chen, S.H. Chen, H.Q. Yang, *Corrosion* 54, 5 (1998): p. 369-376.
25. X.L. Cheng, H.Y. Ma, S.H. Chen, L. Niu, S.B. Lei, R. Yu, Z.M. Yao, *Corros. Sci.* 41 (1999): p. 773-788.
26. X.L. Cheng, H.Y. Ma, S.H. Chen, X. Chen, Z.M. Yao, *Corros. Sci.* 42 (2000): p. 299-311.
27. A. Elbiache, P. Marcus, *Corros. Sci.* 33, 2 (1992): p. 261-269.
28. A.J. Betts, R.C. Newman, *Corros. Sci.* 34, 9 (1993): p. 1551-1555.
29. R.C. Newman, H.S. Isaacs, B. Alman, *Corrosion* 38, 5 (1982): p. 261-265.
30. R.C. Newman, *Corrosion* 41, 8 (1985): p. 450-453.
31. A. Garner, *Corrosion* 41, 10 (1985): p. 587-591.
32. R.C. Newman, W.P. Wong, H. Ezuber, A. Garner, *Corrosion* 45, 4 (1989): p. 282-287.
33. N.J. Laycock, *Corrosion* 55, 6 (1999): p. 590-595.
34. P. Marcus, I. Olefjord, J. Oudar, *Corros. Sci.* 24, 4 (1984): p. 269-278.
35. P. Marcus J.M. Grimal, *Corros. Sci.* 31 (1990): p. 377-382.
36. S. Azuma, H. Tsuge, T. Kudo, T. Moroishi, *Corrosion* 45, 3 (1989): p. 235-242.
37. S. Azuma, T. Kudo, *Corrosion* 47, 6 (1991): p. 458-463.
38. R.P. Case, H.E. Rincon, D.R. McIntyre, *Corrosion* 68, 3 (2012): p. 035004-1 to 035004-12.
39. G. Hinds, L. Wickstrom, J. Abda, A. Turnbull, V. Smith, R. Woollam, *Corros. Sci.* 85 (2014): p. 33-41.
40. ASTM G192, "Standard Test Method for Determining the Crevice Repassivation Potential of Corrosion-Resistant Alloys Using a Potentiodynamic-Galvanostatic-Potentiostatic Technique" (West Conshohocken, PA: ASTM, 2014).
41. ASTM G5, "Standard Reference Test Method for Making Potentiodynamic Anodic Polarization Measurements" (West Conshohocken, PA: ASTM, 2014).
42. T. Okada, *J. Electrochem. Soc.* 131 (1984): p. 1026-1032.
43. D. Rickard, *Geochim. Cosmochim. Acta* 70 (2006): p. 5779-5789.
44. J.F. Zemaitis Jr., D.M. Clark, M. Rafal, N.C. Scrivner, *Handbook of Aqueous Electrolyte Thermodynamics* (New York, NY: American Institute of Chemical Engineers, 1986).
45. M. Rafal, J.W. Berthold, N.C. Scrivner, S.L. Grise, "Models for Electrolyte Solutions," in *Models for Thermodynamic and Phase Equilibria Calculations*, ed. S.I. Sandler (New York, NY: Marcel Dekker, 1995).
46. J.F.J. Zemaitis, *ACS Symposium Series* 133 (1980): p. 227-246.
47. "OLI Analyzer Studio, version 9.2" OLISystems 2015.
48. P. Marcus, E. Protopopoff, *J. Electrochem. Soc.* 137, 9 (1990): p. 2709-2712.
40. P. Marcus, E. Protopopoff, *J. Electrochem. Soc.* 140, 6 (1993): p. 1571-1575.
50. P. Marcus, E. Protopopoff, *J. Electrochem. Soc.* 144, 5 (1997): p. 1586-1590.
51. A. Anderko, P.J. Shuler, *Computers & Geosciences* 23, 6 (1997): p. 647-658.
52. S. Tsujikawa, A. Miyasaka, M. Ueda, S. Ando, T. Shibata, T. Haruna, M. Katahira, Y. Yamane, T. Aoki, T. Yamada, *Corrosion* 49, 5 (1993): p. 409-419.
53. J.R. Galvele, *J. Electrochem. Soc.* 123, 4 (1976): p. 464-474.
54. J.R. Galvele, *Corros. Sci.* 21, 8 (1981): p. 551-579.
55. R.C. Newman, *Interface* 19 (2010): p. 33-38.
56. D.D. Macdonald, *Corrosion* 34, 3 (1978): p. 75-84.
57. R.W. Bosch, W.F. Bogaerts, J.H. Zheng, *Corrosion* 59, 2 (2003): p. 162-171.
58. J. Newman, K.E. Thomas-Alyea, *Electrochemical Systems* (Hoboken, NJ: Wiley, 2004).
59. S.R. De Groot, *Thermodynamics of Irreversible Processes* (Amsterdam, The Netherlands: North-Holland, 1951).
60. J.N. Agar, C.Y. Mou, J.L. Lin, *J. Phys. Chem.* 93, 5 (1989): p. 2079-2082.
61. D.D. Macdonald, A.C. Scott, P. Wentrcek, *J. Electrochem. Soc.* 126, 9 (1979): p. 1618-1624.
62. G.C. Akerlof, H.I. Oshry, *J. Chem. Soc.* 72, 7 (1950): p. 2844-2847.
63. A. Levy, D. Andelman, H. Orland, *Physical Review Letters* 108, 21 (2012): p. 227801.

APPENDIX: CONVERSION OF POTENTIALS OBTAINED USING EXTERNAL SCE ELECTRODE TO THE SHE SCALE

This appendix describes the conversion of a potential measured with respect to an external saturated calomel electrode (SCE) at a temperature T_0, E_{meas}, to the potential of the standard hydrogen electrode (SHE) at the temperature of observation, T, i.e., $E_H(T)$. The solutions in the working and reference vessels are different, i.e., the working vessel contains a NaCl solution of varying concentration, whereas the reference electrode is placed in a saturated KCl solution (4.82 m KCl). The salt bridge between the reference and working vessels contains a NaCl solution with the same concentration as in the working vessel. To make the conversion, it is necessary to estimate the quantity $E_{correction}$ in the relation:

$$E_H(T) = E_{meas} + E_{correction} \quad \text{(A-1)}$$

In order to calculate $E_{correction}$, it is convenient to convert the potential that is measured with respect to the external electrode (i.e., E_{meas}) to a potential relative to SHE at T = 25°C, E_{ext}, i.e., $E_{ext} = E_{meas} + E_{ref,H}(T_0)$, where $E_{ref,H}(T_0)$ is the potential of the external electrode relative to SHE under standard conditions. Thus, for SCE at T_0 = 25°C, the authors have $E_{ref,H}(T_0)$ = 0.2438 V. On the other hand:

$$E_{ext} = E_{WE}(T) - E_{SHE}(T_0) = [E_{WE}(T) - E_{SHE}(T)] + [E_{SHE}(T) - E_{SHE}(T_0)] = E_H(T) + E_{Therm} \quad \text{(A-2)}$$

where $E_{WE}(T)$ is the potential of working electrode. The correction $E_{Therm} = E_{SHE}(T) - E_{SHE}(T_0)$ can be subdivided into two parts, i.e., $= E_{Th,SHE} + E_{TJ}$. The first term, $E_{Th,SHE}$, is the difference between the potentials of two

standard hydrogen electrodes at the temperatures T and T_0 and can be evaluated from a thermodynamic analysis of the cell SHE(298K)SHE(T). Such analysis was performed by Macdonald[56] and Bosch, et al.,[57] and the results can be accurately approximated by:

$$E_{Th,SHE} = 0.8990\times10^{-3}\Delta T - 1.8081\times10^{-6}\Delta T^2 - 1.2589\times10^{-10}\Delta T^3 \quad \text{(A-3)}$$

where $\Delta T = T - 298.15$ K and $E_{Th,SHE}$ is expressed in V.

The second term, E_{TJ}, represents the potential drop in the salt bridge and can be determined experimentally or estimated by considering the mass transfer in the bridge. Such an estimate was developed by assuming that only the NaCl solution is present within the salt bridge and the temperature inside it increases from T_0 to T. On the cold side of the bridge (i.e., near the reference electrode), a thin porous cap separates the saturated KCl and working (NaCl) solutions. The temperature of this cap is equal to that of the reference vessel, i.e., T_0.

Accordingly, E_{TJ} can be in turn subdivided into two parts, i.e., $E_{TJ} = E_{TLJP} + E_{DIF}$, where E_{TLJP} is the potential drop in the salt bridge and E_{DIF} is the potential drop in the porous cap. The latter value can be estimated via the Henderson method.[58] Accordingly, the ion fluxes for i-th species are written in the Nernst-Planck approximation as:

$$J_i = -D_i\nabla C_i - \frac{Fz_iD_i}{RT}C_i\nabla\varphi \qquad i = K^+,\ Na^+,\ Cl^- \quad \text{(A-4)}$$

along with the condition of electroneutrality. In the absence of current, there is $J_{K^+} + J_{Na^+} = J_{Cl^-}$. In addition, in accordance with the Henderson assumption, the concentrations or activities of all species inside the mass transport region (i.e., the porous cap) change linearly.[58] After integration, Equation (A-5) is obtained:

$$E_{DIF} = -\frac{RT}{F}\left[\frac{C_{NaCl}(D_{Na^+} - D_{Cl^-}) - C_{KCl}(D_{K^+} - D_{Cl^-})}{C_{NaCl}(D_{Na^+} + D_{Cl^-}) - C_{KCl}(D_{K^+} + D_{Cl^-})}\right] \ln\left[\frac{C_{NaCl}(D_{Na^+} + D_{Cl^-})}{C_{KCl}(D_{K^+} + D_{Cl^-})}\right] \quad \text{(A-5)}$$

For example, for $T_0 = 25°C$, $C_{KCl} = 4.82$ m, and $C_{NaCl} = 5.7$ m (the latter concentration being considered constant across the bridge because the influence of thermodiffusion on concentration distribution is small), Equation (A-5) yields $E_{DIF} = 4.8$ mV. It should be noted that this is the highest estimate of E_{DIF} for this system. E_{DIF} decreases for smaller NaCl concentrations and, for example, Equation (A-5) yields $E_{DIF} = -0.2$ mV for $T_0 = 25°C$, $C_{KCl} = 4.82$ m, and $C_{NaCl} = 0.44$ m.

The potential drop in the salt bridge E_{TLJP} can be estimated on the basis of the following simplified system of mass transfer equations:[59]

$$J_i = -D_i\nabla C_i - \frac{z_iFD_i}{RT}C_i\nabla\varphi - D_i\sigma_iC_i\nabla T \qquad i = Na^+,\ Cl^- \quad \text{(A-6)}$$

where σ_i are the Soret coefficients. The system (A-6) combines the usual mass transfer equations in the Nernst-Planck approximation with additional thermodiffusional terms. In accordance with Agar, et al.,[60] the Soret coefficient, σ_i, can be expressed as:

$$\sigma_i = \frac{\mathcal{Q}_i^{*0}}{RT^2} = \frac{S_i^*}{RT} = A_i\frac{\partial(1/\varepsilon)}{\partial T} \quad \text{(A-7)}$$

Here $\mathcal{Q}_i^{*0}$ and S_i^* are the ionic heat and entropy of transport, respectively, and ε is the dielectric permeability. In Equation (A-7), the parameter A_i depends on the hydrodynamic radius of the species, which is not well known for any real solution and, hence, should be considered an empirical parameter and derived from experimental data.[60] It was assumed that the parameter A_i only slightly depends on T. When the species fluxes are equal to 0, integration between the points (C^0_{NaCl}, T_0) and (C_{NaCl}, T) yields the following estimate for the thermal liquid junction potential:

$$E_{TLJP} = -\frac{RT}{F}(t_{Na^+} - t_{Cl^-})\ln\left[\frac{C_{NaCl}}{C^0_{NaCl}}\right] - \frac{1}{F}\int_{T_0}^{T}(S^*_{Na^+}t_{Na^+} - S^*_{Cl^-}t_{Cl^-})dT \quad \text{(A-8)}$$

Because the concentration of NaCl inside the salt bridge is approximately constant (i.e., $C_{NaCl} = C^0_{NaCl}$), the first (diffusion) term can be neglected and, in accordance with Equation (A-7) the following is obtained after integration:

$$E_{TLJP} = P\left(\frac{1}{\varepsilon(T)} - \frac{1}{\varepsilon(T_0)}\right) \quad \text{(A-9)}$$

where the parameter P does not depend on temperature. Finally, Equation (A-10) is obtained:

$$E_{correction} = E_{ref,H}(T_0) - E_{Therm} = E_{ref,H}(T_0) - E_{Th,she} - E_{DIF} - E_{TLJP} \quad \text{(A-10)}$$

As shown by Macdonald, et al.,[61] for a KCl salt bridge, E_{TLJP} depends only slightly on concentration in the range $C_{KCl} \le 0.505$ m. Thus, at $C_{KCl} = 0.05$ m, it can be approximated by:[61]

$$E_{TLJP} = 0.842507\times10^{-3}\Delta T - 0.214629\times10^{-5}\Delta T^2 - 0.180993\times10^{-8}\Delta T^3 \quad \text{(A-11)}$$

Equations (A-9) and (A-11) yield very close results (with a deviation of no more than 1 mV to 3 mV) if $\varepsilon(T)$ of pure water is used in Equation (9)[62] and P = 5.7. However, experimental data[63] show that the dielectric constant is reduced by a factor of ~1.7 in nearly

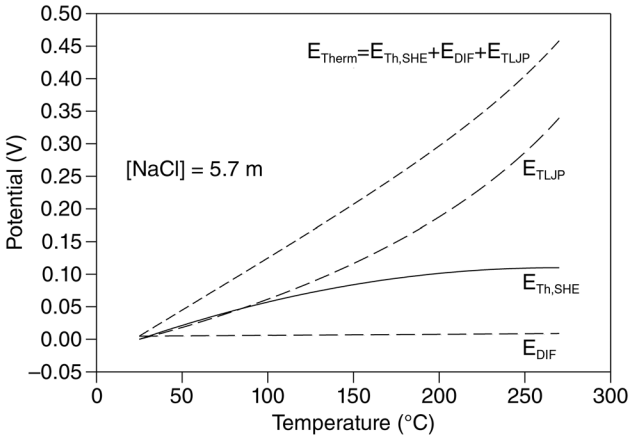

FIGURE A-1. *Correction terms for converting the potential measured with respect to SCE to the SHE scale when the test solution is 5.7 m NaCl.*

saturated KCl solutions at 25°C even though it varies only slightly with concentration for $C_{KCl} \leq 0.505$ m. Although experimental data are not available for ε(T) in saturated KCl at different temperatures, it can be assumed that ε in saturated KCl solutions changes with temperature proportionally to ε in pure water. Then, the parameter P in Equation (9) needs to be changed from 5.7 to 9.9 in order to estimate E_{TLJP} in a saturated KCl solution. It is also natural to observe that, in the case of a NaCl salt bridge, the parameter P must be proportional to the term $(S^*_{Na^+}t_{Na^+} - S^*_{Cl^-}t_{Cl^-})$ instead of the term $(S^*_{K^+}t_{K^+} - S^*_{Cl^-}t_{Cl^-})$ in the case of a KCl salt bridge (cf. Equation [A-8]). Hence, the parameter P will increase for a NaCl salt bridge by the additional factor $\frac{S^*_{Na^+}t_{Na^+} - S^*_{Cl^-}t_{Cl^-}}{S^*_{K^+}t_{K^+} - S^*_{Cl^-}t_{Cl^-}} \approx 1.17$, which is obtained using the entropies of transport at infinite dilution, S^*, according to Agar, et al.[60]

Figure A-1 illustrates the calculated values of $E_{Therm} - E_{SHE}(T) - E_{SHE}(T_0)$ as a function of the temperature drop and shows the contributions of each constituent term when the NaCl concentration in the test solution is 5.7 m NaCl. It should be noted that the dependence of E_{Therm} on NaCl concentration is weak and the behavior shown in Figure A-1 remains valid for other NaCl concentrations.

Finally, the correction term in Equation (A-1) is calculated as:

$$E_{correction} = E_{ref,H}(T_0) - E_{Therm} \quad \text{(A-12)}$$

To facilitate the practical use of Equations (A-1) through (A-12), the correction term can be fitted to the following equations as a function of NaCl concentration:

$$E_{correction}(C_{NaCl}) = E_{correction}(C_{NaCl} = 1m) + b_1 \log C_{NaCl} \quad \text{for } C_{NaCl} \leq 1m \quad \text{(A-13)}$$

TABLE A-1

Parameters Used for Converting the Potentials Measured Using an External Saturated Calomel Electrode (SCE) in a Cooled Luggin Probe to the SHE Scale (cf. Equations [A-13] and [A-14])

t, C	$E_{correction}(C_{NaCl} = 1$ m), V	10^3 b_1, V	10^3 b_2, V/(mol × kg H_2O)
25	0.2429	−1.560	−0.8273
30	0.2349	−1.586	−0.8412
35	0.2270	−1.612	−0.8551
40	0.2190	−1.638	−0.8689
45	0.2111	−1.665	−0.8828
50	0.2032	−1.691	−0.8967
55	0.1953	−1.717	−0.9106
60	0.1874	−1.743	−0.9244
65	0.1795	−1.769	−0.9383
70	0.1715	−1.795	−0.9522
75	0.1636	−1.821	−0.9661
80	0.1557	−1.848	−0.9799
85	0.1478	−1.874	−0.9938
90	0.1398	−1.900	−1.008
95	0.1318	−1.926	−1.022
100	0.1238	−1.952	−1.035
105	0.1158	−1.978	−1.049
110	0.1078	−2.005	−1.063
115	0.0997	−2.031	−1.077
120	0.0916	−2.057	−1.091
125	0.0835	−2.083	−1.105
130	0.0753	−2.109	−1.119
135	0.0671	−2.135	−1.133
140	0.0588	−2.162	−1.146
145	0.0505	−2.188	−1.160
150	0.0421	−2.214	−1.174
155	0.0337	−2.240	−1.188
160	0.0252	−2.266	−1.202
165	0.0166	−2.292	−1.216
170	0.0079	−2.319	−1.230
175	−0.0009	−2.345	−1.244
180	−0.0098	−2.371	−1.257
185	−0.0188	−2.397	−1.271
190	−0.0280	−2.423	−1.285
195	−0.0373	−2.449	−1.299
200	−0.0467	−2.475	−1.313
205	−0.0563	−2.502	−1.327
210	−0.0661	−2.528	−1.341
215	−0.0761	−2.554	−1.355
220	−0.0863	−2.580	−1.368
225	−0.0968	−2.606	−1.382
230	−0.1075	−2.632	−1.396
235	−0.1186	−2.659	−1.410
240	−0.1300	−2.685	−1.424
245	−0.1417	−2.711	−1.438
250	−0.1538	−2.737	−1.452
255	−0.1664	−2.763	−1.466
260	−0.1795	−2.789	−1.479
265	−0.1931	−2.816	−1.493
270	−0.2074	−2.842	−1.507

and

$$E_{correction}(C_{NaCl}) = E_{correction}(C_{NaCl} = 1m) + b_2(C_{NaCl} - 1) \quad \text{for } C_{NaCl} \geq 1m \quad \text{(A-14)}$$

The parameters of Equations (A-13) and (A-14) have been tabulated as a function of temperature in Table A-1.